Seismic Earth Pressure Analysis Against a Rigid Wall Undergoing Various Modes of Movement Based on Coupled Shear Band Method

Hemanta Hazarika, School of Engineering, Nagoya University

INTRODUCTION

In the earthquake prone zones, proper estimation of the seismic earth pressure against retaining structures assumes significant importance, especially in the vicinity of port facilities where high intensity earthquakes can cause damage to the retaining structures resulting in catastrophe to the adjoining infrastructures and consequently to the human lives. The Great Hanshin Earthquake on 17th January, 1995 in Japan, in which Kobe port was badly damaged, serves as a stark reminder to both the research and the planning community the enormity of the damage caused by a devastating earthquake and it's repercussions on social and economic front. Thus, the zones frequented by seismic activities need adequate earthquake resistant design. The huge damages to the retaining walls during the Great Kanto Earthquake in Japan, 1926 gave a wake up call to the research community in the field of earth pressure, leading to the well known Mononobe-Okabe theory which is extensively used till date for the seismic design of the retaining structures.

The Mononobe-Okabe theory is based on the classical Coulomb theory which has intrinsic fallacies brought to light by Terzaghi in 1936. It assumes the pressure distribution to be hydrostatic, a fact which is hardly demonstrated by the experimental observations. In addition, the retaining wall can undergo various kinds of movement depending on the situations and the earth pressure distribution pattern (Fig. 1) depends on these modes resulting in differences in the values of the resultant thrust as well as it's point of application. For example, when relatively deep fills or adjacent structures exist in front of the toe section of a retaining wall, the passive earth pressure from the fills or the adjacent structures prevent the movement of the wall at the lower portion of the wall. In this case the wall undergoes rotational movement about the base (RB). On the other hand, for bridge abutments, only the lower portion can move since the outer movement at the top is restrained by the relatively rigid superstructures. In such situations, the mode of displacement is rotation about the top (RT). In Fig. 1, the two aforementioned modes are shown for the active displacement of the wall.

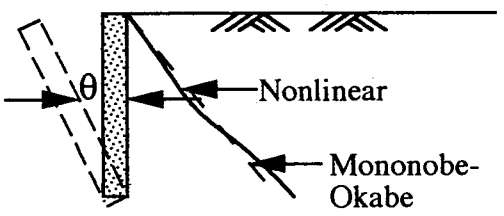

(a) Rotation about base (**RB**)

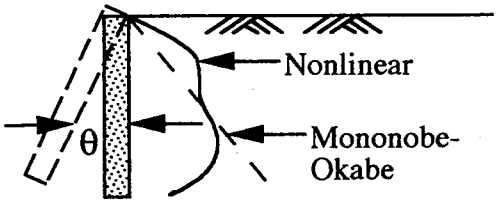

(b) Rotation about top (**RT**)

Fig. 1 Wall Movement Modes

Experimental researches on the wall movement modes dependent seismic earth pressure were performed by various researchers (Ohara(1970), Ichihara and Matsuzawa (1973), Sherif, Ishibashi and Lee (1982), Ishibashi and Fang (1987)). However, numerical model to simulate this dependency and thus translate the results into the design is still at it's infancy. Although analytical expressions have been put forward (Saran and Prakash (1977), Dimarogona (1983)) to explain the nonlinear distribution for various wall movement modes, those are not seen to suffice in explaining the exact nature of distribution as they can not truly capture the progressive nature of deformation of the backfill. Hence the development of an efficient numerical model is deemed necessary for the analyses of seismic earth pressure that will be able to capture the progressive failure. This research is a step forward in that direction.

When deformed sufficiently into the plastic range, deformation within granular materials such as sand tends to concentrate along bands called shear bands resulting in non-uniform stress state. Element possessing such shear bands has been named as *cracked element* by Kawamoto and Takeda (1979). The generated shear band is known to be a factor responsible for the strain softening characteristics of the material, which significantly affects the predicted limit load. In the case of granular soil, the slip surface develops progressively within the ground. Thus, simultaneous mobilization of the peak strength at various location of the slip surface will be rarely encountered. Hence the numerical analysis of the progressively deforming material calls for the consideration of the shear bands within an element. Progressive failure analyses such as earth pressure analysis should take into account the effects of the incepted shear bands. Above all, the earth pressure phenomenon is more likely to undergo shear band bifurcation, as the plane strain condition is quite sensitive to the localized shearing.

The primary objective of this research is to develop a numerical methodology for the seismic analyses of a retaining wall-backfill system that includes the effect of the shear bands during the deformation process of the backfill and apply this methodology to explain the generation of the seismic active earth pressure against a rigid wall undergoing various modes of movement. The elements undergoing localized shearing are modeled incorporating two shear bands and the constitutive relation, named here as *Coupled Shear Band Method*, is formulated by coupling the two bands. An experimental model is simulated in the analyses and the efficacy of the developed method is demonstrated by comparing the results of the analyses with the experimental observations as well as the analytical solutions put forward by Dimarogona (1983).

FORMULATION OF COUPLED SHEAR BAND METHOD

Once localized shearing takes place, the post bifurcation behavior can be idealized as pseudo-uniform deformation using smearing technique (Pietruszczak and Mroz (1981), Pietruszczak and Stolle (1987)). Pietruszczak and Mroz (1981) introduced the smeared shear band theory to model the localized elements using only one shear band. However, theoretical background supports the existence of two bands along which the strain is localized. It is also shown experimentally that if co-axiality of the ends of the sample is imposed by the apparatus, generally two shear bands will be observed crossing each other (Desrues, 1990). Therefore, for an element with localized strain the constitutive description should incorporate the effect of both the bands.

Constitutive Relation

Considering a triangular element, at the instant of inception of the shear bands, the element can be assumed to be composed of three sub-elements as shown schematically in Fig. 1. Such an element will be called *Cracked Triangular Element*. The strain rates generated inside each sub-element are also shown in the figure. The inclinations θ_1 and θ_2 of the two bands with the X axis are given by the Coulomb orientation

$$\theta_1 = \theta^1 - \left(\frac{\phi}{2} + \frac{\pi}{4}\right); \qquad \theta_2 = \theta^1 + \left(\frac{\phi}{2} - \frac{3\pi}{4}\right) \tag{1}$$

where θ^1 is the angle from X axis to the major principal axis and ϕ is the angle of internal friction.

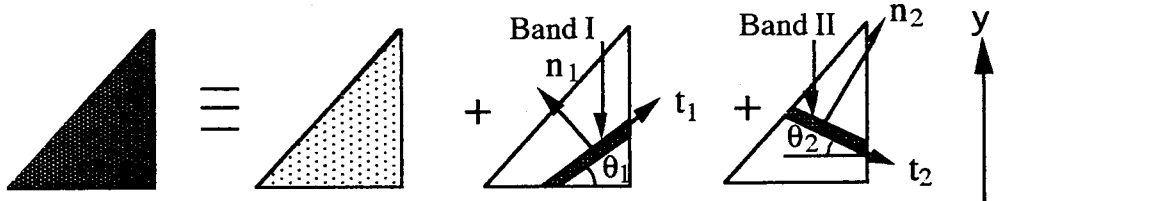

Fig. 2 Cracked Triangular Element with Two Shear Bands

Considering finite deformation within the band, the constitutive relations for the two bands are given by the following relations in the {x,y} coordinate system

$$\text{Band I:} \quad \bar{\mathbf{d}}_1 = \frac{1}{H}[\bar{C}_1]\hat{\sigma}_1; \qquad \text{Band II:} \quad \bar{\mathbf{d}}_2 = \frac{1}{H}[\bar{C}_2]\hat{\sigma}_2 \tag{2}$$

in which $\bar{\mathbf{d}}$ and $\hat{\sigma}$ represents the rate of deformation tensor and the Jaumann rate of stress tensor respectively and H is the softening modulus. $[\bar{C}_1]$ and $[\bar{C}_2]$ are the compliance matrices in the {x, y} coordinate system for the band I and the band II respectively. Expressing $\hat{\sigma}_1$ and $\hat{\sigma}_2$ in terms of Couchy's stress rate $\dot{\sigma}$ and then some transformations render the following equations

$$\bar{\mathbf{d}}_1 = \frac{1}{H}([I] - \frac{1}{H}[\bar{C}_1]\beta\delta_1{}^T)^{-1}[\bar{C}_1]\dot{\sigma} \tag{3}$$

$$\bar{\mathbf{d}}_2 = \frac{1}{H}([I] - \frac{1}{H}[\bar{C}_2]\beta\delta_2{}^T)^{-1}[\bar{C}_2]\dot{\sigma} \tag{4}$$

in which $\mathbf{I}$ is the unit tensor and β is given by the expression

$$\beta = \{-2\sigma_{xy}, 2\sigma_{xy}, (\sigma_x - \sigma_y)\}^T \tag{5}$$

δ_1 and δ_2 are the transformation matrices defined by the orientation angles θ_1 and θ_2 and can be obtained by substituting the values of θ in the expression given below

$$\delta = \{-sc,\ sc,\ \frac{1}{2}(c^2 - s^2)\}^T \tag{6}$$

where $s = \sin(-\theta)$; $c = \cos(-\theta)$. Introducing the smearing factor ζ defined to be the ratio of the area of the shear band to the area of the element, the infinitesimal plastic strains in the two sub-elements can be expressed as

$$\dot{\varepsilon}_1^P = \zeta\bar{\mathbf{d}}_1 \tag{7}$$

$$\dot{\varepsilon}_2^P = \zeta\bar{\mathbf{d}}_2 \tag{8}$$

Substituting Eqs. (3) and (4) into Eqs. (7) and (8) and then using Fig. 1 the constitutive law takes the form

$$\dot{\varepsilon} = \{([I] - \frac{1}{H}[\bar{C}_1]\beta\delta_1{}^T)^{-1}[\bar{C}_1] + ([I] - \frac{1}{H}[\bar{C}_2]\beta\delta_2{}^T)^{-1}[\bar{C}_2] + \frac{H}{\zeta}[C^e]\}\frac{\zeta}{H}\dot{\sigma} \tag{9}$$

in which C^e is the elastic part of the compliance matrix obtained using Young's modulus E and Poisson's ratio ν. Eq. (9) represents the constitutive relations for the cracked elements. The constitutive relation for the non localized elements is given by the conventional relation for elasto-plastic strain hardening material with the yield function and the plastic potential function represented by Eq. 10 discussed in the following subsection. For simplicity, isotropic hardening/softening is assumed in the formulations that follow.

Hardening and Softening Modulus

The yield function f and the plastic potential function g during hardening are assumed to be given by the following Mohr-Coulomb criterion with the major principal stress, σ_1 and the minor principal stress, σ_3

$$f = (\sigma_1 - \sigma_3) + (\sigma_1 + \sigma_3)\kappa\ ; \qquad g = (\sigma_1 - \sigma_3) + (\sigma_1 + \sigma_3)\eta \tag{10}$$

where κ and η are the hardening function and the dilatancy parameter respectively which are assumed as

$$\kappa = \frac{\kappa_f\xi}{A + \xi}\ ; \qquad \eta = \frac{\kappa - \kappa_c}{1 - \kappa\kappa_c} \tag{11}$$

in which κ_f is a constant representing failure, A is the material constant, ξ is the plastic distortion and κ_c is a constant defining the zero dilatancy state. The consistency condition yields the hardening modulus H as

$$H = -(\sigma_1 + \sigma_3)\frac{\kappa_f A}{(A+\xi)^2} \tag{12}$$

The yield function f_b and the plastic potential function g_b inside the bands in the {n,t} coordinate system are assumed as

$$f_b = \sigma_{nt} + \kappa_s \sigma_n \; ; \qquad g_b = \sigma_{nt} + \eta_s \sigma_n \tag{13}$$

where κ_s is the softening function assumed to be given by (Pietruszczak and Stolle, 1987)

$$\kappa_s = \eta_s \{1 + \exp[-R(\gamma^p - \gamma_0)]\} \tag{14}$$

where η_s is the dilatancy parameter, R is the material constant that determines the rate of softening, γ^p is the plastic shear strain that accumulates within the band after it's inception and γ_0 is the value of shear strain when $\gamma^p = 0$. Using the above yield and plastic potential functions, the softening modulus can be obtained from the consistency condition as

$$H = R\sigma_n(\kappa_s - \eta_s) \tag{15}$$

MODEL SIMULATION AND METHOD OF ANALYSES

The *Coupled Shear Band Method*, discussed in the preceding section is applied to simulate an experimental research on the wall movement modes dependent dynamic active earth pressure. As of the present, the application is restricted only to the experimental model, since the idea is to develop a fundamental method through simulation of the model tests to examine the efficiency of the method, instead of directly applying it to the field problems which have no reliable data. The University of Washington's shaking table and retaining wall assembly (Ishibashi and Fang, 1987) has been employed in the simulation. The finite element discretization of the model with CST elements is shown in Fig. 3. Interface elements reported in Ref. 3 are incorporated between the wall and the backfill to simulate the wall friction.

The wall movement modes (RB and RT) shown in Fig. 1 are considered in the analyses. The analyses are performed in time domain using Wilson's theta method to calculate the applied dynamic increment on the model retaining wall. The Updated Lagrangian formulation is used in the stress-strain calculations. The material parameter values of the backfill sand used/assumed in the analyses are given in Table 1.

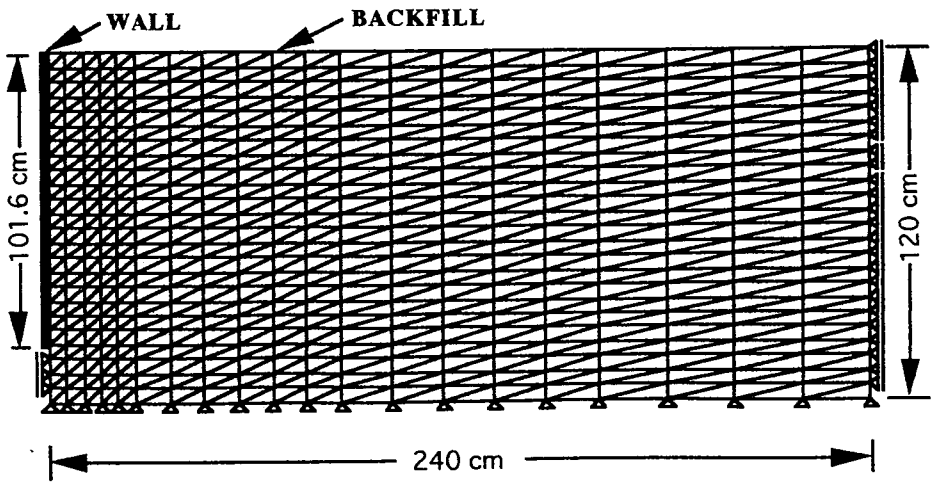

Fig. 3 Finite Element Discretization of the Experimental Model *(Not to the scale)*

RESULTS AND DISCUSSIONS

Earth Pressure Distribution and the Active State

For the retaining walls and similar structures, the action of the earthquake is the most dangerous when the horizontal acceleration is directed towards them. Hence practically, it is sufficient to consider only the effect of the maximum inertia force. Figs. 4(a) and 4(b) show the distributions of the horizontal earth pressure with depth z, at different wall rotations for the RB mode and the RT mode respectively in the case of maximum inertia force. From the results, it can be observed that the distribution pattern depends on the mode of movement of the wall and is highly nonlinear. The noticeable points in the figures are the earth pressure at the top and the base of the wall. In the case of the RB mode, the earth pressure decreases faster at the top, while for the RT mode, the earth pressure shows an increase in value with increasing deformation. On the other hand, at the base portion of the wall, while the RB mode shows existence of higher stress, the RT mode exhibits rapid reduction of stress. This is due to the different mechanism of deformation resulting from differences in stress conditions for each case. The progressive nature of the failure pattern of the backfill elements is responsible for this difference in the mechanism of deformations.

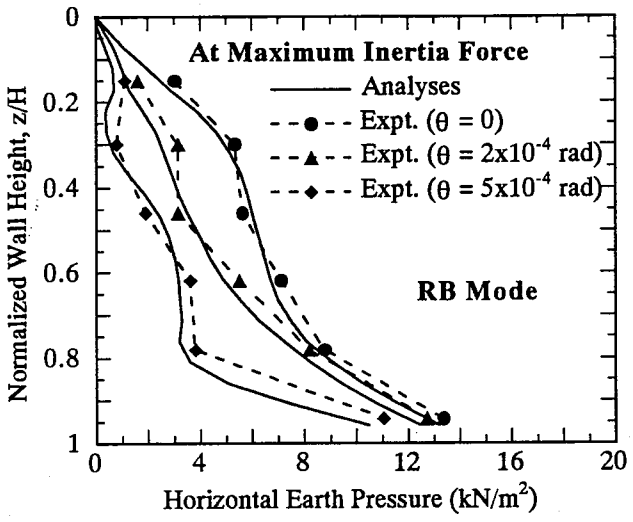

(a) Rotation about Base (RB) Mode

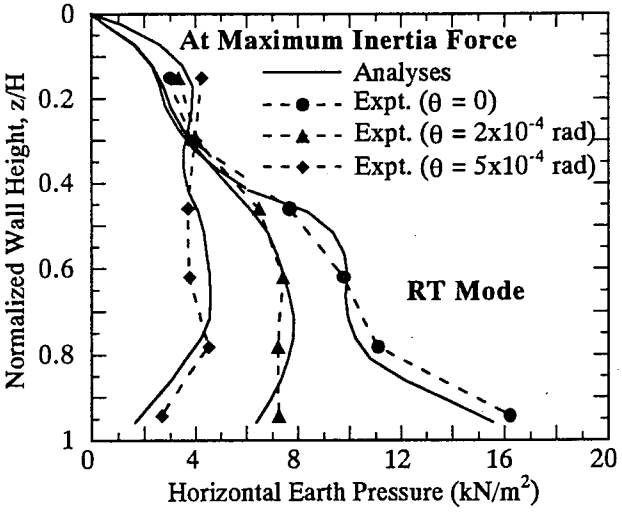

(a) Rotation about Top (RT) Mode

Fig.4 Distribution of Horizontal Earth Pressure with Wall Rotation

Table 1. Material Parameters of Backfill

Parameters	Values
Young's Modulus E (kN/m^2)	21000
Poisson's Ratio ν	0.3
Friction Angle ϕ	40.1^0
Deformation Parameters	
A	0.0037
R	0.05
κ_f	0.427
Dilatancy Parameters	
κ_c	0.454
η_s	0.510
Smearing Parameter	
ζ	0.4×10^{-5}

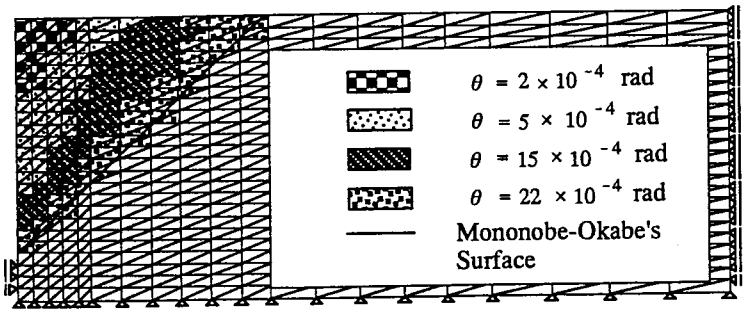

(a) Rotation about the base (**RB**) Mode

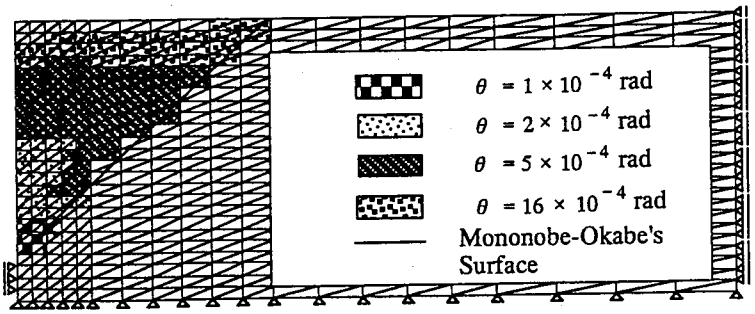

(b) Rotation about the top (**RT**) Mode

Fig. 5 Progressive Failure Pattern of the Backfill Elements

Figs. 5(a) and 5(b) show the progression of the localized zone with cracked elements at various values of the wall rotation when subjected to an acceleration of 200 gals. In the case of the RB mode, as can be seen in Fig. 5(a), the failure starts from the top and advances towards the base of the wall, finally forming a clear active wedge of Rankine type. However, for the RT mode (Fig. 5(b)), the failure initiates at the base and moves towards the backfill surface. In this case, elements at the top never reached the failure state. This can be attributed to the arching phenomenon which dominates the backfill surface near the wall for this mode of movement. These two figures explain the phenomenon observed in Figs. 4(a) and 4(b); the early failed backfill elements contribute to the reduction of stress for both the modes, while arching phenomenon contributes to the higher stress at the top for the RT mode. The extra higher stress at the base for the RB mode comes from the restriction of the movement of the backfill at the base. The stage when the backfill forms a failure wedge consisting of elements with localized strain can be defined as the active state since even with further movement of the wall the progression ceases. Mononobe-Okabe's failure surface using constant angle of internal friction ϕ is also shown in the figures. It is to be noted that the elements touched by the Mononobe-Okabe's surface are having different mobilized angles of internal friction at that stage.

Figs. 6(a) and 6(b) show the distributions of the horizontal thrust at the active state for the two modes. The pattern of the distribution curves obtained from the analyses shows reasonable agreement with the experimental trend. For comparison, the active state distribution obtained from Dimarogona's analytical expression is also plotted in the figures along with Mononobe-Okabe's hydrostatic distribution. Dimarogona's method can only qualitatively express the nonlinear characteristics of the active thrust distribution and it's dependency on the wall movement modes.

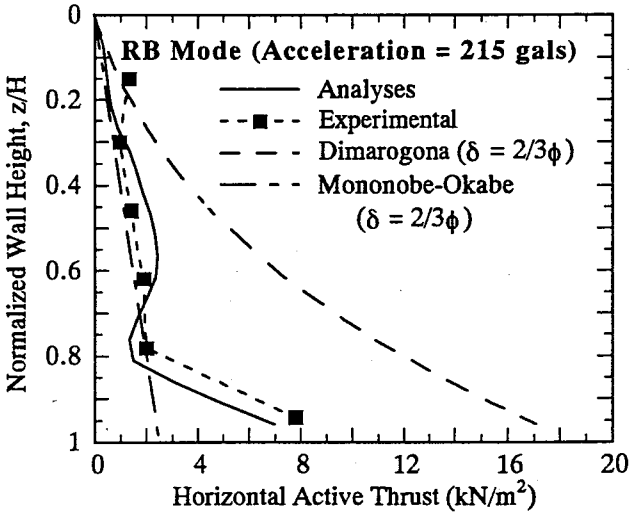

(a) Rotation about Base (RB) Mode

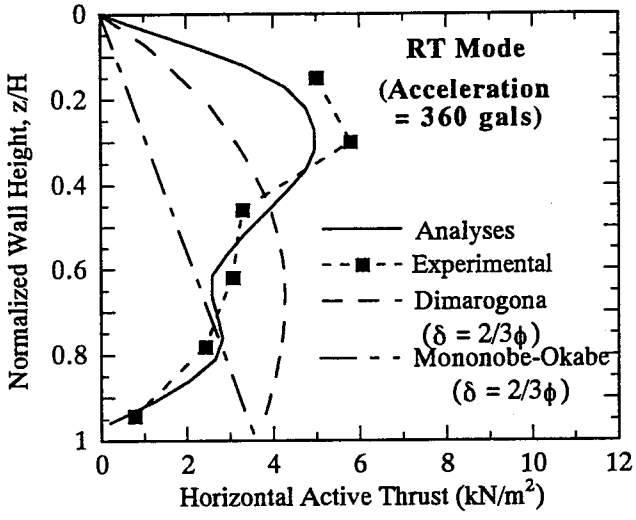

(a) Rotation about Base (RB) Mode

Fig. 6 Seismic Active Earth Pressure Distribution for Each Mode of Movement

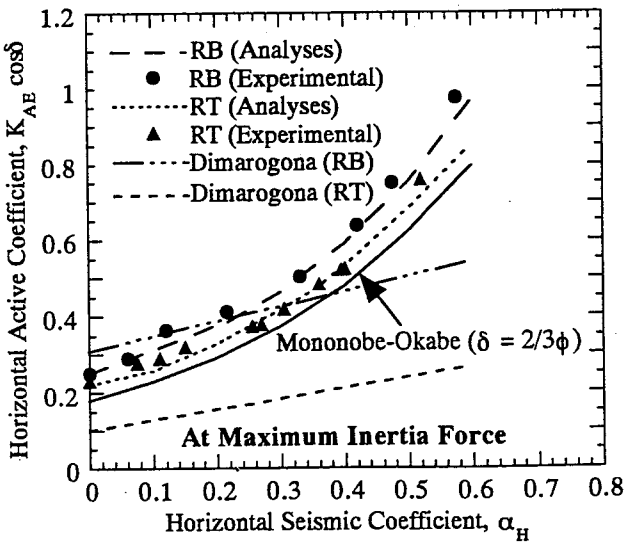

Fig. 7 Variation of K_{AE} with Seismic Coefficient

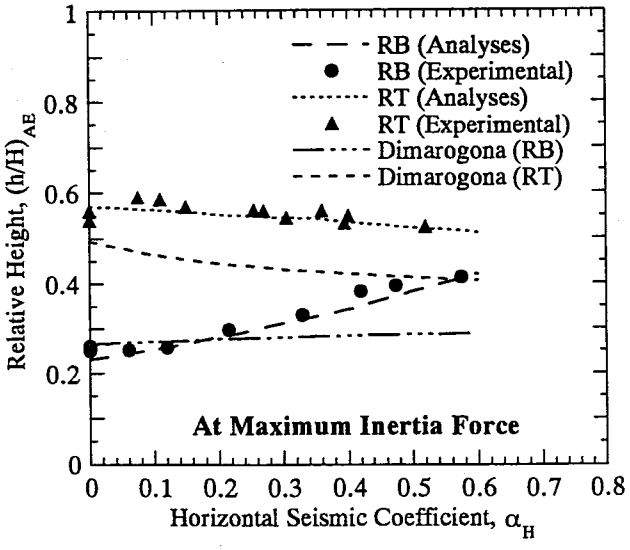

Fig. 8 Variation of $(h / H)_{AE}$ with Seismic Coefficient

Fig. 7 shows the variations of the horizontal component of the coefficient of seismic active thrust K_{AE} as a function of horizontal seismic coefficient, α_H along with the experimental values, Mononobe-Okabe's values as well as the values given by Dimarogona's method. It can be seen that the RB mode gives the highest and the RT gives the lowest value of K_{AE}. While the analyses could explain the experimental trend satisfactorily, Dimarogona's method fail to carry any weight quantitatively, which may be due to the fact that the method can not truly capture the progressive failure of the backfill with the movement of the wall.

Fig. 8 shows the relations between the relative height of point of application of the resultant active thrust, $(h / H)_{AE}$ and α_H, where H is the height of the wall. A trend similar to the experimental results can be observed, that is, for the RB mode $(h / H)_{AE}$ increases with acceleration, while for the RT mode it decreases. Dimarogona's method for RB mode shows negligible increase of the value with accelerations.

Increment of Dynamic Active Thrust and It's Point of Application

The issue of the incremental dynamic active thrust and it's point of application still remains controversial in the field of dynamic earth pressure. Ichihara and Matsuzawa (1973) assumed that the dynamic increment of active thrust can be given by an equivalent surcharge whose point of application acts at the midheight of the wall. Sherif et. al. (1982) found from their experiments that the dynamic increment acts at 0.48H from the base of the wall. However, according to Seed and Whitman it acts at the height of 0.6H. Therefore, it is the need of the time to elucidate the truth regarding this.

Fig. 9 shows a conceptual drawing used to calculate the total seismic active earth pressure. Generally, the incremental dynamic thrust ΔP_{AE} is calculated by using the theory of elasticity, which is not a justified concept for the earth pressure calculations. Therefore, ΔP_{AE} and it's point of application need to be judged based on the calculations using plasticity theory.

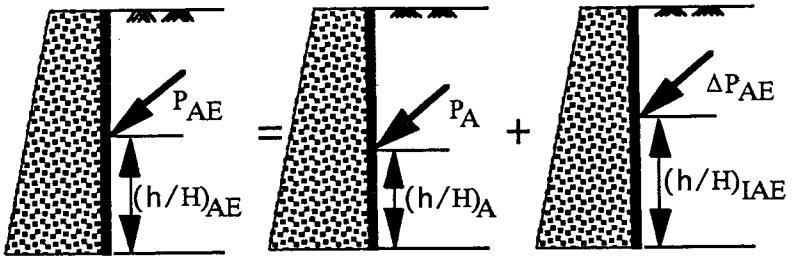

Fig. 9 Illustration of the Dynamic Increment

Fig. 10 shows the relations between the calculated incremental horizontal coefficient of seismic active thrust, ΔK_{IAE} and α_H for the two modes. The relationships exhibit a nonlinear pattern for both the modes, with the RB mode giving a higher value of ΔK_{IAE}. Similar relationships (Fig. 11) for the relative height of the incremental active thrust, $\Delta(h / H)_{IAE}$ reveal that the RB mode results in lower and the RT mode results in higher value of $\Delta(h / H)_{IAE}$ at lower acceleration levels. However, at higher level of acceleration, the values cluster around 0.5 which coincides with the recommendation of Ichihara and Matsuzawa. It can be inferred from this observation of the numerically calculated values that at the higher acceleration levels the wall movement modes do not effect the point of application of the dynamic increment.

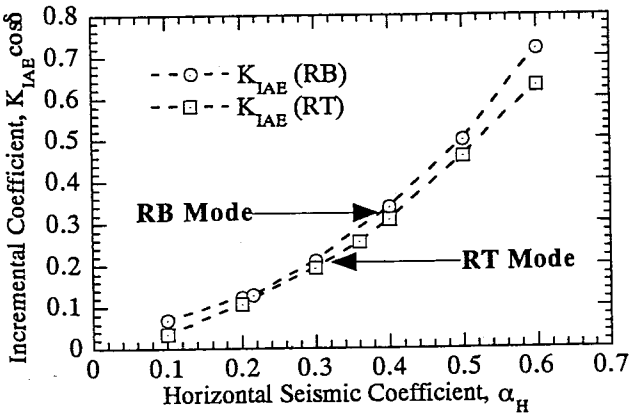

Fig. 10 ΔK_{IAE} Vs. Horizontal Acceleration

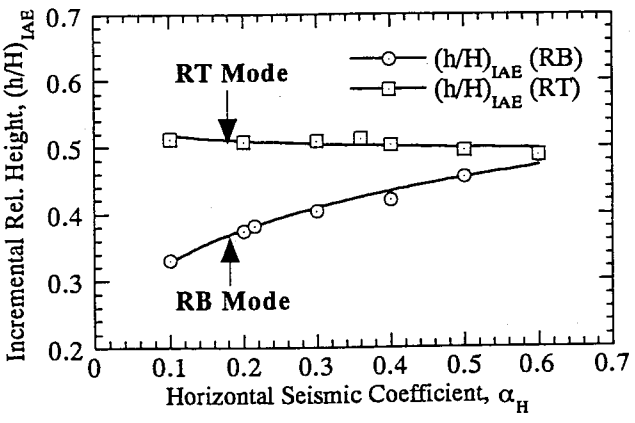

Fig. 11 $\Delta(h / H)_{IAE}$ Vs. Horizontal Acceleration

CONCLUDING REMARKS

The *Coupled Shear Band Method* presented in this paper can adequately capture the progressive deformation characteristics of the sandy backfill behind a rigid retaining wall undergoing various modes of displacement. The numerical analyses based on this method lead to the following conclusions.

1) The progressive failure pattern of the backfill exhibits different behavior depending on the wall movement modes resulting in the differences in the earth pressure distributions.

2) The failure zone progression lead to the formation of the active wedge. As a result, the values of the active state parameters such as, the coefficient of the seismic active thrust, it's point of application and their increments differ depending on the modes of movement of the wall.

3) The point of application of the dynamic increment of the earth pressure is not significantly affected by the wall displacement modes at the higher acceleration levels.

ACKNOWLEDGMENT

The author would like to thank Dr. Hiroshi Matsuzawa of Ohyo Corporation Ltd., formerly Associate Professor in the Department of Geotechnical and Environmental Engineering, Nagoya University for his guidance in conducting this research.

REFERENCES

[1] Desrues, J. (1990), "Shear Band Initiation in Granular Material: Experimentation and Theory", In Geomaterials: Constitutive Equations and Modelling, Ed. F. Darve, Elsevier Applied Science, London, pp. 283-310.

[2] Dimarogona, P.D. (1983), "Distribution of Lateral Earthquake Pressure on a Retaining Wall", Soils and Foundations, Vol. 23, 4, pp. 1-10.

[3] Hazarika, H., Matsuzawa, H. and Sugimura, M. (1995), "The Influence of Interface Behavior on Dynamic Earth Pressure Analyses", Chubu Regional Conference of JSCE, Nagoya, pp. 357-358.

[4] Ichihara, M. and Matsuzawa, H. (1973), "Earth Pressure During Earthquake", Soils and Foundations, Vol. 13, 4, pp. 75-86.

[5] Ishibashi, I. and Fang, Y.S. (1987), "Dynamic Earth Pressure with Different Wall Movement Modes", Soils and Foundations, Vol. 27, 4, pp. 11-22.

[6] Kawamoto, T. and Takeda. N. (1979), "An Analysis of Progressive Failure in Rock Slopes", 3rd Intl. Conf. on Num. and Anal. Meth. in Geomech., Aachen, Vol. 2, pp. 797-808.

[7] Ohara, S. (1970), "Experimental Studies on Seismic Active and Seismic Passive Earth Pressure", The Third Japan Earthquake Engineering Symposium, pp. 137-144.

[8] Pietruszczak, S. and Mroz, Z. (1981), "Finite Element Analysis of Deformation of Strain Softening Materials", Intl. Journ. of Num. Meth. in Engg., Vol. 17, pp. 327-334.

[9] Pietruszczak, S. and Stolle, D.F.E. (1987), "Deformation of Strain Softening Materials, Part II:", Computers and Geotechnics, Vol. 4, pp. 109-123.

[10] Prakash, S. (1981), "Analysis of Rigid Retaining Walls During Earthquakes", Intl. Conf. on Recent Advances in Geotechnical Earthquake Engineering and Soil Dynamics, Missouri, Vol. 3, pp. 993-1019.

[11] Saran, S. and Prakash, S. (1977), "Effect of Wall Movement on Lateral Earth Pressure", The Sixth World Conference on Earthquake Engineering, New Delhi, India, Vol. 3, pp. 2371-2372.

[12] Sherif, M.A., Ishibashi, I. and Lee, C.D. (1982), "Earth Pressure against Rigid Retaining Walls", Journal of the Geotechnical Engineering Division, ASCE, Vol. 108, GT5, pp. 679-693.